Scientific Research Publishing

World Journal of Engineering and Technology, 2024, 12, 117-140
https://www.scirp.org/journal/wjet
ISSN Online: 2331-4249
ISSN Print: 2331-4222

Effect of Spray Rails on Takeoff Performance of Amphibian Aircraft

Soham S. Bahulekar, Alberto W. Mello*

Embry-Riddle Aeronautical University, Daytona Beach, Florida, USA
Email: *melloa2@erau.edu

How to cite this paper: Bahulekar, S.S. and Mello, A.W. (2024) Effect of Spray Rails on Takeoff Performance of Amphibian Aircraft. *World Journal of Engineering and Technology*, **12**, 117-140.
https://doi.org/10.4236/wjet.2024.121008

Received: December 16, 2023
Accepted: February 5, 2024
Published: February 8, 2024

Abstract

Amphibian aircraft have seen a rise in popularity in the recreational and utility sectors due to their ability to take off and land on both land and water, thus serving a myriad of purposes, such as aerobatics, surveillance, and firefighting. Such seaplanes must be aerodynamically and hydrodynamically efficient, particularly during the takeoff phase. Naval architects have long employed innovative techniques to optimize the performance of marine vessels, including incorporating spray rails on hulls. This research paper is dedicated to a comprehensive investigation into the potential utilization of spray rails to enhance the takeoff performance of amphibian aircraft. Several spray rail configurations obtained from naval research were simulated on a bare Seamax M22 amphibian hull to observe an approximate 10% - 25% decrease in water resistance at high speeds alongside a 3% reduction in the takeoff time. This study serves as a motivation to improve the design of the reference airplane hull and a platform for detailed investigations in the future to improve modern amphibian design.

Keywords

Seaplane, Spray Rails, Hull Optimization, Take-Off Performance

1. Introduction

Seaplanes, especially modern amphibian aircraft, are fixed-wing aircraft that can take off and land on water. They can be classified into float planes and flying boats [1]. Float planes have floats or pontoons attached to aircraft with conventional fuselage. Common examples of floatplanes include Aviat Husky and Viking DHC-6 Twin Otter. Some of them are easy to convert from conventional aircraft to their amphibian counterpart but sacrifice performance due to the floats' added weight. Flying boats have a hull blended with the fuselage designed

for water operations [1]. Since they are designed from the ground up with specific missions in mind, in terms of performance and reliability, flying boats are more versatile and capable than floatplanes. The PBY Catalina, Lisa Akoya, Icon A5, and Seamax M22 are some examples of flying boats.

Nowadays, the appeal of seaplanes is more aligned with recreation and adventure due to low operating costs and ease of flying. The Icon A5, Lisa Akoya, and Seamax M22 are examples of sport-based amphibians serving the recreational and thrill-seeking demographic. Moreover, the demand for amphibians is rising for utility purposes like firefighting and surveillance. A good example is the DHC-515 Firefighter. This multi-purpose amphibian is well-equipped to attack wildfires that are more prevalent these days due to climate change [2].

Flying boat hulls generate more drag and perform at lower speeds than conventional aircraft for similar missions [1]. Therefore, seaplane design requires a good balance between aerodynamics and hydrodynamics. Since the focus of the design is directed toward the hydrodynamics of amphibians, it is imperative to understand the features of the hull and their function. As shown in **Figure 1**, the keel of the hull aids in guiding the seaplane along a straight line [1]. The seaplane is centered at the keel in terms of lateral stability. The front end of the hull is the bow, while the rear end is the step. The step introduces a discontinuity between the hull and the tail end of the seaplane (or the stern) to ensure rotation during takeoff [1]. Chines are referred to as the seams of the hull located at the sides. However, with the introduction of chine strips that extend from the seams, they are considered a separate addition to any watercraft and have become quite common in modern amphibians. When the hull moves on water, it generates water spray, which can cause water to reach components such as the cockpit, landing gear hub, cabin air inlets, and cargo compartments. The water spray is incredibly destructive to kick-back propellers, which reduces the power efficiency of the amphibian. Water spray on the cockpit causes low pilot visibility during takeoff. Moreover, it can cause water logging in otherwise dry components, which could corrode them, reducing the amphibian's lifespan.

Spray rails aid in the suppression of water spray. Located at strategic locations under the hull and below the chines, they help keep water at bay by deflecting it as soon as it touches the hull [3]. The spray rails break the edge into smaller edges, reducing the overall water spray [4] [5]. The spray edge is formed at the front of the stagnation line, highlighted in **Figure 2**. The spray rails break the spray edge into smaller edges, reducing the overall water spray. Furthermore, spray rail additions reduce the wetted-area width of the hull, thus reducing resistance [6] [7]. While spray rails are beneficial in reducing the water spray on the cockpit and propeller, it can increase noise during hydroplaning, compromising the ride's awareness during takeoff [4]. Moreover, adding spray rails and chines would increase production and labor costs [4]. Therefore, using an optimal number of spray rails is essential to balance reducing water spray and achieving a smooth and comfortable ride.

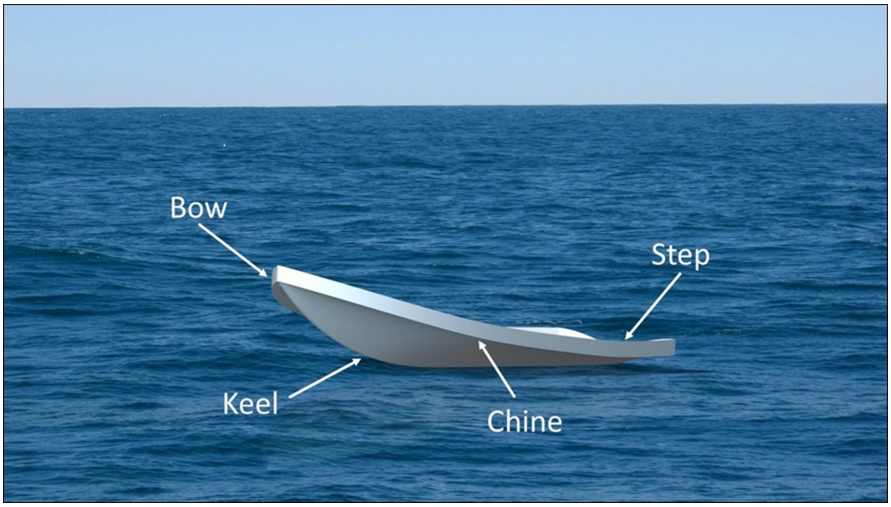

Figure 1. Visual representation of an amphibian hull.

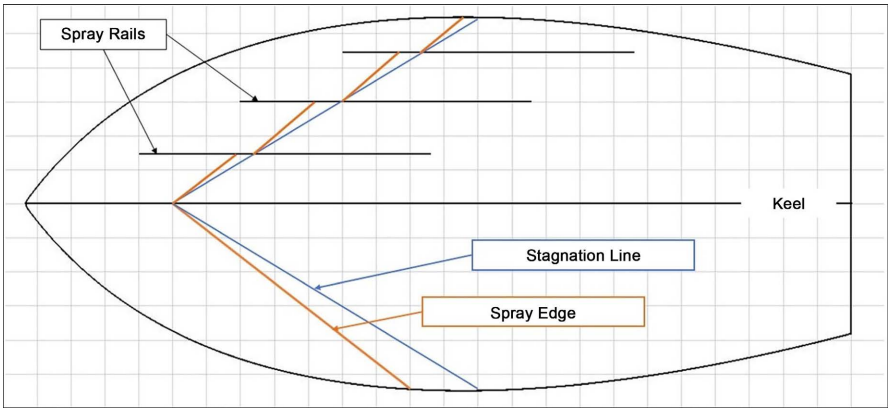

Figure 2. Water spray prediction with (top) and without (bottom) spray rails below an amphibian hull.

Incorporating chines and spray rails in hull design has long been regarded as beneficial for the above reasons. However, apart from previous hull models and test data for mostly large boats and ships, no conclusive study has explored their optimal design [4]. Recent naval studies have tested different spray rail configurations with varying design parameters like angle and width, which have not been applied extensively to amphibians yet. This paper explores these unanswered topics and focuses on the influence of spray rails on the takeoff distance and time and serves as a starting point for future studies on improved design.

2. Literature Review and Theoretical Framework

In the late 1940s, the focus on designing flying boats and amphibians shifted from military applications to recreation and transportation. At the time, many studies proposed and tested various hull models to form a database for seaplane manufacturers, the most notable being the hydrodynamic investigation of amphibian hull models by Hugli and Axt [8]. Results like water resistance, spray height, and lateral and longitudinal stability were recorded for each hull model.

In addition, differences were found between unflared and flared hulls; flaring refers to the curvature from the keel to the chine edge of the hull. That and increased deadrise forebody and after body warping provided better hydrodynamic characteristics [8]. In addition, some comparisons were made between conventional and planing tail hulls. Conventional hulls have a step from the hull afterbody to the tail, whereas planing hulls have a blended tail. Planing hulls were designed to increase hydroplaning characteristics to reduce air drag, water resistance, and increase stability [9]. Modern amphibians have planing hulls with flared bottoms and increased deadrise warping for these advantages. Another notable observation by Hugli and Axt was that hydrodynamic parameters like resistance can be scaled from hull models through a linear factor, which can be obtained by comparing design geometric parameters. This concept will be explained further and utilized for this study. Until the early twenty-first century, amphibian research mainly focused on the shape optimization of hull models for amphibians, while the idea for any external hull modifications to reduce water spray remained unexplored.

Spray rails garnered interest in naval architecture in the 1960's. Clement [10] studied the effects of spray rails on resistance for large boats and ships by fitting spray rails with different length variations and their effects on resistance and water spray deflection. A 6% decrease in resistance at high speeds (known as planning phase, to be defined later) was discovered for the limited-length rails, with no increase recorded for low speeds (displacement phase). Clement explored the difference between rounded and sharpened edges as well. Sharpened edges presented a resistance of 1.5% lower than rounded edges [10]. While this may seem a slight improvement, a future study by Savitsky *et al.* in 2007 validated that sharp rails cause the water spray to detach faster than round rails because the water spray was found to attach to the round edge [11]. Although Clement highlighted the importance of the length and location of the spray rails, variations in spray rail geometry were not discussed, such as the shape and deflection angle.

Müller-Graf *et al.* [6] proposed a similar experiment in 1991, where spray rail configurations that differed in length, width, height above the waterline, number of rails, and deflection angle were created and tested at semi-displacement speeds to curb the unnecessary increase in resistance at those speeds as presented by Clement [10]. They proposed some general requirements for optimal spray rails, which are still considered by hull designers today. It was found that the spray rails can generate additional lift to the hull, useful for quicker hydroplaning and decreasing resistance due to the smaller immersed volume of the hull [6]. Another revelation was that the number of spray rails and deflection angle are essential in reducing the hull's wetted surface area. Spray flow patterns suggested that the spray rail amount should be increased if the water spray reattached itself to the hull after deflection [6]. Less wetted surface area in addition to a 2˚ - 10˚ increase in deflection angle with respect to the waterline, reduced the hull's resistance by up to 8%, compared with the bare hull resistance for one

spray rail [6]. Müller-Graf *et al.* work was well received and regarded by the naval and oceanography communities as the only systematic investigation of spray rails until today [4]. A recent study by Lakatoš *et al.* in 2021 backed the cumulative research done by Clement and Müller-Graf by introducing their spray rail configurations with varying spray rail geometry for planing hulls [4]. These studies covered the hydrodynamic effects of spray rails on hulls used for boats, yachts, and ships, but the knowledge of such spray rails being attached to amphibian hulls is still relatively unknown.

While it is true that studies on spray rails were inclined more toward naval architecture, a couple of studies have taken initiatives in implementing spray rails to amphibian hulls. In 2013, Frediani *et al.* performed a preliminary Computational Fluid Dynamics (CFD) analysis on a new ultralight amphibious aircraft termed 'IDINTOS' [12]. In this research project, they introduced a spray rail along each side of the hull bottom to observe the changes in takeoff performance. They validated Müller-Graf *et al.*'s findings by showing that spray rails reduce the wetted area of the hull, which provides better pilot visibility [6] [12]. This substantiates that water spray over the cockpit is a problem that amphibian aircraft have been facing, which can be minimized by adding spray rails. Moreover, a high-fidelity CFD analysis was performed to test the proposed amphibian's hydrodynamic performance, highlighting the importance of planing hulls over conventional hulls, the effects of step height, CG location and step planform angle [12]. Water tank tests were performed to ensure the hydrodynamic changes can be predicted in full-scale models. Their research findings corroborated the work done by Hugli and Axt [8] and by Suydam [9] in the 1950s, where the CFD analyses validated the need for a linear scaling factor to be used for water tank tests for larger-scale models. In addition, water tank tests proved to be a better platform than CFD to narrow down and select hull configurations; CFD was merely used to initiate a preliminary design for a new amphibian [12]. However, the variation of spray rail geometry was still unexplored, what is a motivation for the current study.

To understand the effects of water spray on takeoff performance, one must be introduced to the basics of hydrodynamics and the parameters that directly affect the water spray on the amphibian aircraft. Firstly, the load or the buoyant force on water, as found from the Archimedes principle, is defined to be [1]:

$$\Delta = w\nabla = \rho_w g\nabla \tag{1}$$

The load Δ is typically the gross weight of the seaplane, and the specific weight $w$of fresh water is 9786.5 N/m^3 (62.3 lb/ft^3) [8]. The displaced volume ∇ refers to the volume moved by the seaplane. Buoyancy relates to the floating tendency of the seaplane, which greatly contributes to the hydrostatic stability and overall water displacement during movement [1]. The non-dimensional term for the load is given by:

$$C_\Delta = \frac{\Delta}{wb^3} \tag{2}$$

being b the maximum beam length as previously defined. The speed coefficient can represent the speed of the seaplane:

$$C_V = \frac{V}{\sqrt{gb}} \tag{3}$$

where v is the speed, and g is the acceleration due to gravity (9.81 m/s^2 or 32.2 ft/s^2). The Froude displacement number $F_{r\nabla}$ is like the speed coefficient but is a function of the displaced volume by the hull rather than the beam length. The displaced volume is a better parameter as it focuses on the effects of the overall shape and size of the hull and not just one geometric parameter.

$$F_{r\nabla} = \frac{V}{\sqrt{g\nabla^{1/3}}} \tag{4}$$

When a seaplane moves on the water, it encounters water resistance R as the opposing force to thrust in addition to some air drag. Resistance at low speeds also affects water spray, as less resistance allows for reduced water displacement. The resistance coefficient is defined as:

$$C_R = \frac{R}{wb^3} \tag{5}$$

During a takeoff run, the seaplane undergoes three phases of motion: displacement, transition (hump), and planning [13]. In the displacement phase, skin friction and water spray mainly contribute to the water resistance, although the skin friction factor can be omitted due to flying boat convention [14]. Buoyancy is also a factor here; the floating tendency affects how long the seaplane will be in the displacement phase during the run. The coefficient of resistance in this phase can be defined as a function Φ of speed and load [14]:

$$\frac{C_R}{C_\Delta^{2/3} C_V^2} = \Phi\left(\frac{C_V^2}{C_\Delta^{1/3}}\right) \tag{6}$$

As the name suggests, the transition or hump phase sets up the transition from displacement to the planning phase. The resistance peaks during the takeoff run at the "hump". The planning phase, short for hydroplaning, sees a reduction in resistance due to the seaplane relying on dynamic lift [14]. The resistance is simplified because the Froude displacement number becomes less important in this phase [14]:

$$\frac{C_R}{C_V^2} = \Phi\left(\frac{C_\Delta}{C_V^2}\right) \tag{7}$$

Figure 3 provides a representation of the different phases of motion during a takeoff run. Based on the behavior of the resistance curve, it is possible to predict the range of the different phases. **Table 1** shows the phases in terms of Fr_∇ [4]. The resistance curve is plotted as R/Δ vs Fr_∇ to show the resistance changes non-dimensionally, the focus remains on the relative changes in resistance rather than the actual values. It is observed that the resistance increases steeply during the displacement range and reaches its maximum value at the hump

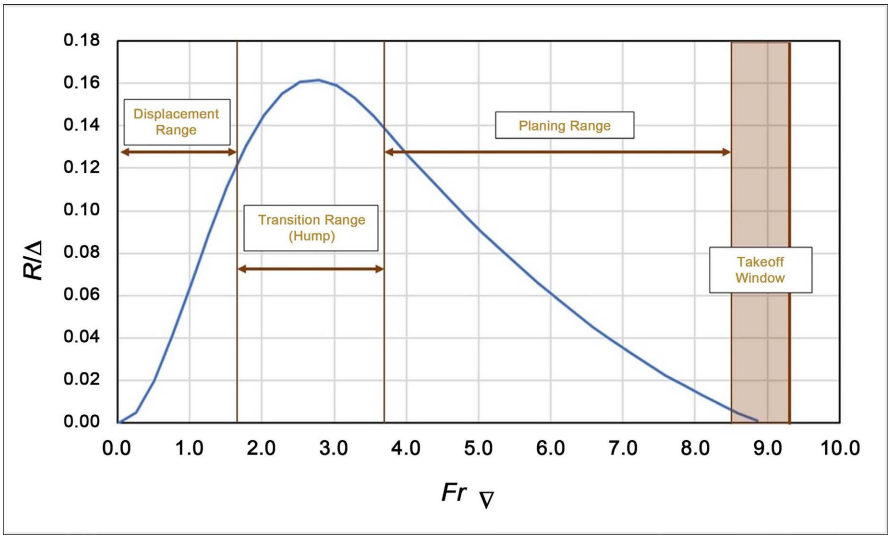

Figure 3. Non-dimensional resistance curve of a seaplane during a takeoff run.

Table 1. Froude displacement number range during takeoff run.

Phase	Fr_{∇}
Displacement	<1.75
Transition (Hump)	1.75 - 3.5
Planing	>3.5

range. This is where the amphibian hull displaces the water to the side and generates a wake at the step. The resistance drops gradually at the planing range, where the hull starts hydroplaning, thus generating lift. The resistance becomes zero once the amphibian takes off, so the speed associated with this is the takeoff speed of the amphibian.

The trim angle governs the longitudinal orientation of the seaplane. A smooth rise in trim ensures good longitudinal stability during the takeoff run. A 2˚ increase in trim angle throughout the takeoff run is required for planning hulls for ease [1]. An approximation of the trim angle curve for planing hulls is shown below in Equation (8) [1], and its evolution during takeoff depicted in **Figure 4**.

$$\tau = \tau_1 + \frac{(\tau_2 - \tau_1)}{2}\left(1 + \tanh\left(A_\tau C_V + B_\tau\right)\right) \tag{8}$$

$$A_\tau = \frac{5.294}{(C_{V2} - C_{V1})} \tag{9}$$

$$B_\tau = -\left(2.647 + A_\tau C_{V1}\right) \tag{10}$$

The trim angles τ_1 and τ_2 are at the start and end of the takeoff run, respectively. The speed coefficients C_{V1} and C_{V2} correspond to the trim angles τ_1 and τ_2. C_{V2} is assumed to be the speed coefficient where the resistance of the hull is maximum or when the seaplane begins to hydroplane since the orientation of the hull given by τ_2 needs to be constant at the planning phase [1] [9].

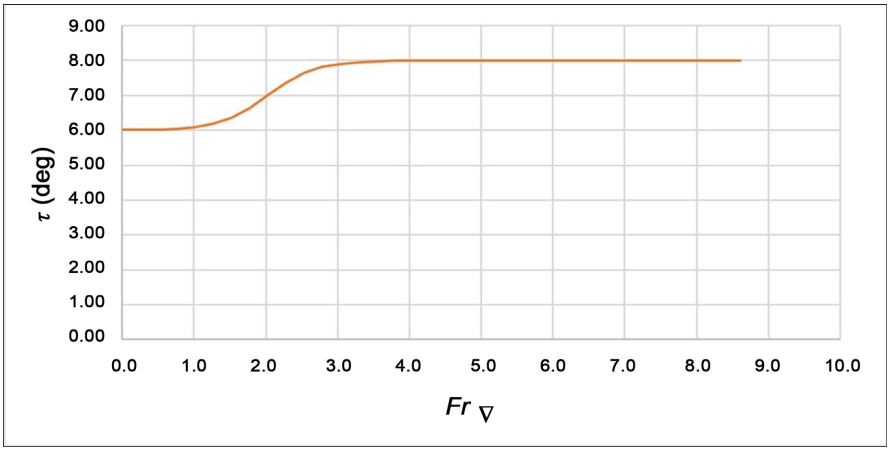

Figure 4. Calculated trim angle of a seaplane during a takeoff run.

It is important to note that this approximation is for calm water conditions and that factors like rocky waves and crosswinds will affect the trim angle because it is directly related to the stability of the seaplane.

The water spray can be assumed as a spray blister curve that originates at the stagnation line, which is the maximum spray wave that can be generated by the hull [15]. Water spray occurs mainly in the displacement range, as waves are created when the hull starts to move through the water. This causes water to splash over the cockpit, which affects pilot visibility. In addition, water spray accounts for about 10% of the overall resistance [4] [11] [16]. Hence, it is vital to lower the water spray, which will inevitably reduce the resistance and improve the takeoff performance of the amphibian.

Specific guidelines must be observed for spray rail design. A spray rail consists of these critical parameters: angle (δ), width (b_{SR}), and length (L_{SR}). The measurement of the spray rail angle, δ, as illustrated in **Figure 5**, is taken from the deflecting edge of the spray rail to the lateral water line. This Figure shows five typical rail configurations and how to determine the rail angle and width based on its basic geometry. The deadrise angle is defined by the angle formed between the water line and the closest straight streamline following the hull. Spray rails reduce the deadrise angle locally and increase buoyancy as illustrated in **Figure 6** and explained by Lakatoš *et al.* [4]. However, excessive reduction in the deadrise angle can cause the hull to porpoise. Porpoising is a form of dynamic instability that occurs during hydroplaning, which is a coupled oscillation in pitch and heave of the hull, as reported by Celano [17]. Porpoising can cause a rough ride as well as severely damage the structural integrity of the hull [3]. Additionally, this angle must not surpass the perpendicular orientation of the lateral water line, as such an occurrence could induce the development of a vortex at the intersection between the spray rail and the hull, as dictated by fluid dynamics. Hence, achieving an optimal spray rail angle is essential to minimize water spray disruption and maintain an appropriate level of lift.

Müller-Graf *et al.* [6] developed a systematic analysis of the shape, size, and location of spray rails for low-speed watercraft $\left(Fr_{\nabla} < 1.0\right)$ and recommended

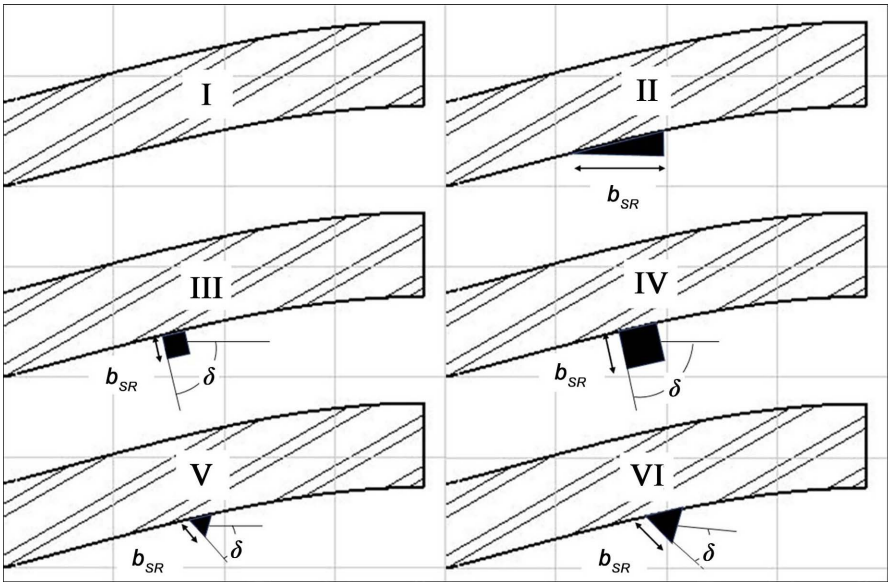

Figure 5. Illustration of amphibian hulls with no rail (I) and five spray rail configurations (II - VI).

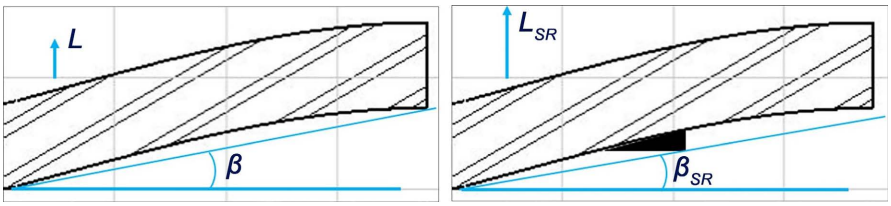

Figure 6. Effect of spray rails on deadrise angle and lift.

that the spray rail width be 0.5% of the length of the waterline. Also, the spray rails must begin forward of the stagnation line to deflect initial spray at displacement speeds. These can extend to the step at high-speed operations to prevent chine walking, the phenomenon where the hull raises from the step [18]. While this harbors a concern for high-speed planning boats, this could benefit seaplanes since the goal is to takeoff from the water as soon as possible. Thus, the length and location of the spray rail is essential.

Another important parameter is the length of spray rails. The spray rails extending to the step can break the water spray formed around the stagnation line during planning speeds. Short spray rails are effective to do so during displacement phase but will not avoid spray in the last stage of the takeoff run. Figure 7 illustrates this phenomenon with hypothetical stagnation lines drawn where they should occur, and two different sets of spray rails for comparison. The stagnation line moves to the rear of the hull as speed increases. Short rails, in the top of the figure, and long rails in the bottom. Spray rails must be sharp at the outer edge and blended into the hull smoothly [10] [18]. If the spray rail's outer edge is rounded, it can cause the spray sheet to remain attached to the deflection surface, thus preventing the ability to deflect the water spray [11]. The amount of spray rails mounted on the hull is another important factor. Typically, the

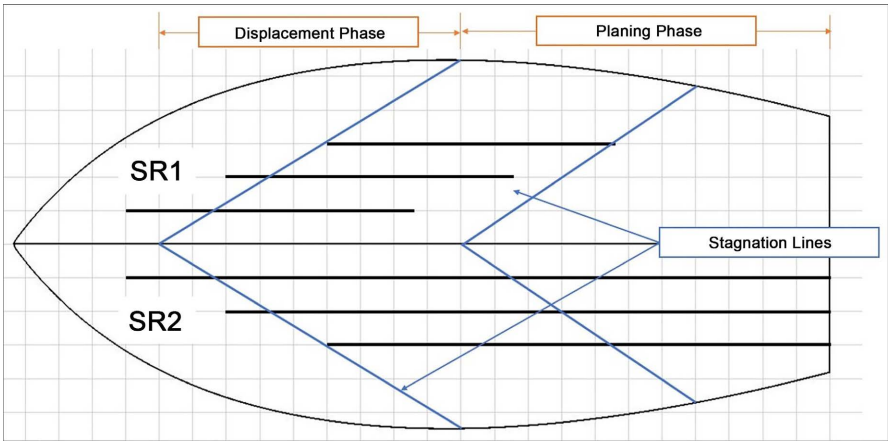

Figure 7. Spray rail lengths and the impact in the stagnation lines at different takeoff phases. Top (SR1)—short rails, bottom (SR2)—long rails.

amount of spray rails is decided based on the spray pattern. Müller-Graf *et al.* [6] stated that the water spray must be detached from the spray rails without reattaching further aft of the hull. Staggering multiple spray rails achieves this condition, where the spray rail begins at the start of the water spray and ends where the spray starts to reattach to the hull, which acts as the starting point for the next spray rail.

Lakatoš *et al.* [4] provided some applicable spray rail configurations that vary in angle and width. These configurations are tested on the bare hull configuration adapted from Seamax M22 [19]. We have defined spray rail configurations as SR1 for short spray rails, and SR2 for long spray rails as depicted in **Figure 7**. The width of the spray rails is formulated in terms of b_{SR}/L_{WL} as a percentage [4]. As previously defined, the angle of the spray rail δ is defined as the angle between the water surface and the bottommost edge of the spray rail. The conventional spray rails have a horizontal deflection surface, *i.e.*, $\delta = 0^{\circ}$. The chosen width percentage for this study is at the recommended limit as previously mentioned $\left(b_{SR} = 11.5 \text{ mm}\right)$. The small and large spray rails refer to their relative size, where the large spray rails are 0.2% larger than the small ones. Cases III, IV, VII, and VIII have a rectangular cross-section, while V and VI have a triangular cross-section, as seen in **Figure 5**. The shapes were chosen to reflect the deflection angle and the sharpness of the spray rails; evidently, the triangular cross-section has a lesser deflection angle but is sharper than the rectangular cross-section. Moreover, according to Lakatoš *et al.* [4], the manufacturing process for these spray rails was easy due to their simplistic shapes. **Table 2** briefly describes the spray rail configurations selected for this study.

At this point, the main objective is to close the gap from previous studies by introducing concepts that align with naval architecture. The focus ison the hydrodynamics of the seaplane during takeoff, with the seaplane hull adapted from the Seamax M22 aircraft as a proof of concept. **Table 3** provides a summary of design parameters that will be used for the takeoff performance analysis:

Table 2. Summary of spray rail configurations.

Case	Description	b_{SR}/L_{WL} (%)	δ (deg)
I	Bare Hull	-	-
II	SR1 – Conventional	0.5	0
III	SR1 – Small Rectangular	0.1	-70
IV	SR1 – Large Rectangular	0.3	-70
V	SR1 – Small Triangular	0.1	-25
VI	SR1 – Large Triangular	0.3	-25
VII	SR2 – Small Rectangular	0.1	-70
VIII	SR2 – Large Rectangular	0.3	-70

Table 3. Summary of design parameters.

Parameter	Imperial		Metric	
Δ	1320	lb	5871.6	N
β	20	deg	20	deg
b	3.6	ft	1.1	m
b_s	2.5	ft	0.76	m
L_f	9	ft	2.74	m
L_{WL}	7.5	ft	2.29	m
w	62.3	lb/ft^3	9786.5	N/m^3
g	32.2	ft/s^2	9.81	m/s^2
τ_1	6	deg	6	deg
τ_2	8	deg	8	deg

The design parameters in Table 3 will be used to determine the hull's water resistance, trim and spray location based on model test data obtained from references [8] and [14] and will be considered as the benchmark. The spray rail configurations will induce changes in hydrodynamic performance during takeoff, represented by comparing the resistance, trim, and spray.

Our main hypotheses are that adding spray rails should reduce the time required for takeoff by lowering the hull's resistance while maintaining longitudinal and lateral stability. Although the takeoff time could be reduced, the takeoff speed should remain the same once it is an aerodynamic condition for the flight phase. The longitudinal stability will not change significantly, which can be checked by the changes in the trim angle. The hull's resistance must have a smooth and gradual decrease during hydroplaning to show that no porpoising effects occur.

3. Methodology

The takeoff performance is broken down into the following parameters: resis-

tance, trim, and spray location. As highlighted previously, these parameters will be compared for different spray rail configurations. Since resistance plays a vital role in the takeoff performance of a seaplane, it will be the resulting parameter for comparison. The resistance data was obtained by scaling the M22 using a linear scaling factor λ, which was found as a result of a geometric mean of several linear scaling factors relating to the geometric parameters of the model. **Table 4** summarizes the data used for the determining the linear factor by finding the geometry mean.

The resistance and speed of the bare M22 hull can be scaled using the following equations [5]:

$$R = R_{f_M}\lambda^{2.7} + R_{d_M}\lambda^{3} \tag{11}$$

$$V = V_M\lambda^{0.5} \tag{12}$$

R_f is the frictional resistance, R_d is the dynamic resistance, and the subscript 'M' denotes the model data. To analyze the changes in resistance by the different spray rail configurations, some necessary curve-fitting equations were found for each phase of motion for the bare hull configuration based on charts presented by Hugli and Axt [8]:

$$R/\Delta = -0.0283Fr_\nabla^3 + 0.0917Fr_\nabla^2 - 0.00002Fr_\nabla \left(\text{Displacement}\right) \tag{13}$$

$$R/\Delta = 0.0055Fr_\nabla^3 - 0.0741Fr_\nabla^2 + 0.2814Fr_\nabla - 0.1662\left(\text{Hump}\right) \tag{14}$$

$$R/\Delta = 0.0025Fr_\nabla^2 - 0.0581Fr_\nabla + 0.3195\left(\text{Planning}\right) \tag{15}$$

The SR1 and SR2 configurations will provide a change in the resistance curve during planning speeds [4] [10]:

$$\delta R = 2.4586Fr_\nabla^2 - 29.824Fr_\nabla + 78.716 \ \left(\text{SR1}\right) \tag{16}$$

$$\delta R = 0.83Fr_\nabla^2 - 15.293Fr_\nabla + 45.156 \ \left(\text{SR2}\right) \tag{17}$$

The drag D and thrust T during takeoff can be scaled to fit using the following equations [1]:

$$D = \frac{0.0259V^2 + 0.0433V + 0.8}{1.467} \tag{18}$$

$$T = T_{72\%} - 2.172V \tag{19}$$

Under the assumption that Seamax M22 operates at 72% of the maximum continuous power for takeoff in calm water, it was found that $T_{72\%}$ = 1788 N (402 lb) [19] [20]. The time required for takeoff was chosen to represent potential changes in takeoff performance. The total takeoff time is calculated by dividing the takeoff range into small segments and by numerically integrating the times for each segment for the complete takeoff range. The total takeoff time can be found using the following equations:

$$t = \sum_{i=1}^{n} \frac{V_{i+1} - V_i}{a_i} \tag{20}$$

Table 4. Determination of linear factor.

Linear Parameters (ft)	Model	Seamax M22	Linear Factor
b	0.50	3.6	7.2
b_s	0.50	2.5	5.0
L_f	1.6	9	5.5
L_a	1.7	6.8	4.0
h_s	0.042	0.32	7.7
Final linear factor (λ)			**5.7**

$$a_i = \frac{g\left[T-\left(R+D\right)\right]}{\Delta} \tag{21}$$

where a_i is the average acceleration in the i^{th} segment. Equations (20) and (21) show that the takeoff time is related to the resistance. For different spray rail configurations, changes to the resistance will be observed, affecting the takeoff time.

The takeoff analysis shall have some constraints for realistic results. The main parameters for the current analysis to be used as a proof of concept will be: seaplanes' takeoff time must be less than 60 seconds [1]. Since the hull analysis is performed using Seamax M22 as reference, the takeoff speed must be between 55 - 60 mph [19]. The trim angle must be stable at planning speeds ($F_{r\nabla} > 3.5$) to prevent hull porpoising and slamming [1] [9]. The number of spray rails must not exceed 6 to avoid additional labor costs and counter productivity, wherein more spray rails will increase resistance due to added weight and flow separation, causing a turbulent wake [3] [4]. The spray rails should be evenly spaced with respect to the beam length to avoid any flow irregularities. As stated by Müller-Graf [6], $b_{SR}/L_{WL} \le 0.5\%$ is the optimal width condition, which will be another constraint. The length of the rails should be well within the step and the location of the stagnation line [4]. Finally, since the spray should be deflected downward and to the sides of the hull, the angle of the spray rails should be between 0° and -90° [4] [11].

4. Results

4.1. Water Resistance

The following results are obtained by analyzing the configurations describe in Table 2. Applying all the conditions and restrictions quantified by the equations defined in the previous chapter, the non-dimensional resistance R/Δ for the displacement phase (Figure 8) and hump phase (Figure 9) could be obtained as a function of the Froude displacement number Fr_∇. The bare hull configuration will be considered as the benchmark for comparison. Compared to the bare hull, the general trend is that the resistance increases by about 2% - 7% at displacement speeds, while the increase drops down to about 1% - 4% at hump speeds with the addition of spray rails. Figure 10 shows the cases for the planning

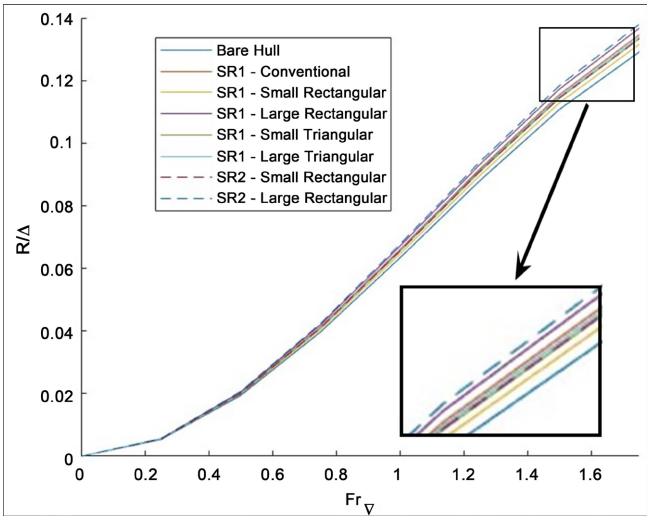

Figure 8. Water resistance at displacement speeds.

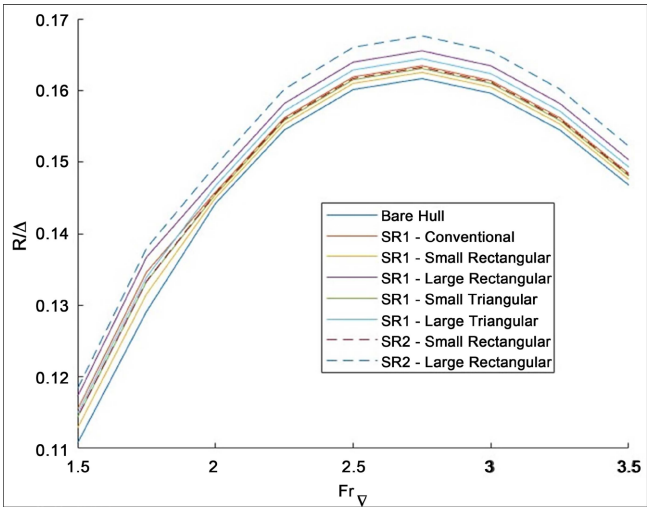

Figure 9. Water resistance at hump speeds.

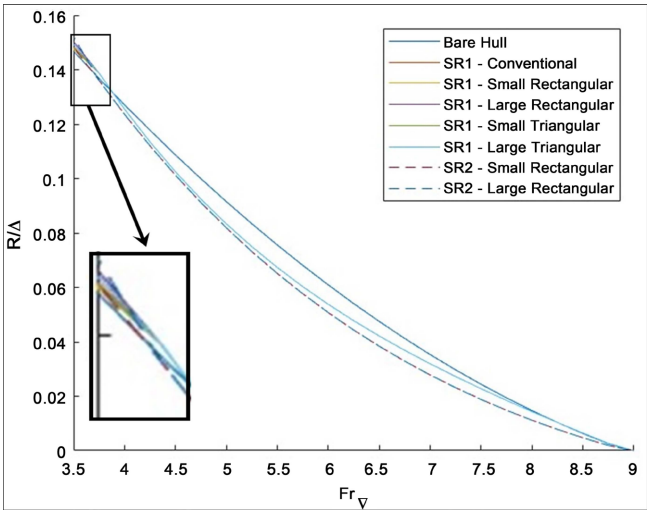

Figure 10. Water resistance at planing speeds.

phase. In this stage, the curves begin to converge as speed approaches takeoff speed, although there is a clear indication that SR1 and SR2 are distinguishable from each other. During hydroplaning, the spray rails reduce the water resistance by about 10% - 25%, which is relatively significant compared to the resistance change observed at displacement and hump speeds.

Table 5 summarizes the maximum variation for the resistance in the displacement and hump phases.

4.2. Trim

Figure 11 shows the trim angle τ as a function of Froude displacement number Fr_{∇}. The trim angle curves were observed diverge at hump speeds to reflect the changes in trim due to the addition of spray rails. At displacement speeds, the change in trim is relatively significant, causing a maximum of 0.2˚ positive deflection from the benchmark, recorded by Case IV (SR1 – Large Rectangular) spray rails. This deflection reduces to 0.1˚ at the start of the planing speed and remains constant throughout. Table 6 provides the maximum trim deflections for all cases.

4.3. Takeoff Time

As covered in the previous chapter, the takeoff times were computed for each spray rail configuration. To portray that the computed takeoff times vary with angle and width, they were interpolated to obtain a series of takeoff times against the width ranging from 0.1% to 0.3%, and the angle ranging from 0˚ to 70˚. As a result, the surface plots were generated. Figure 12 is the surface plot for all SR1 configurations, whereas Figure 13 is the surface plot for all SR2 configurations. Table 7 summarizes the computed takeoff times for the different spray rail configurations. The optimal angle was 50.2˚ for short spray rails and 70˚ for long. The optimal width was 0.17% of the length of the waterline $\left(b_{SR} = 3.9 \text{ mm}\right)$, which was typical for both SR1 and SR2. These optimal points are plotted at the lowest takeoff time.

5. Discussion

The takeoff time was reduced by 2% with the addition of short spray rails, whereas a 3% reduction was found for long spray rails. This reduction is expected to increase for larger hulls with larger wet areas. The 20˚ deadrise angle (Table 3) is quite low, which could be unaffected even after the addition of spray rails because they produce additional lift by reducing the deadrise. A more drastic change could have been seen if the deadrise angle had been more significant. As analyzed by Clement [10], a deadrise angle larger than 20˚ could have different hydrodynamic effects. However, modern amphibians have deadrise angles of less than 20˚, so the additional lift generated by attaching spray rails could be negligible.

The resistance changes caused by the optimal spray rails could hold merit as they affect the water spray created by the hull. Figure 14 plots the resistance

Table 5. Change in resistance at displacement and hump speeds.

Case	Description	δR (%) [Displacement]	δR (%) [Hump]
I	Bare Hull	0	0.000
II	SR1 – Conventional	4.256	1.105
III	SR1 – Small Rectangular	1.884	0.537
IV	SR1 – Large Rectangular	5.872	2.395
V	SR1 – Small Triangular	3.217	0.860
VI	SR1 – Large Triangular	3.718	1.710
VII	SR2 – Small Rectangular	3.291	0.971
VIII	SR2 – Large Rectangular	6.839	3.688

Table 6. Maximum deflection in trim at hump speeds.

Case	Description	$\delta\tau$ (deg)
I	Bare Hull	0.000
II	SR1 – Conventional	0.133
III	SR1 – Small Rectangular	0.106
IV	SR1 – Large Rectangular	0.198
V	SR1 – Small Triangular	0.090
VI	SR1 – Large Triangular	0.164
VII	SR2 – Small Rectangular	0.079
VIII	SR2 – Large Rectangular	0.180

Table 7. Takeoff times for different spray rail configurations.

Case	Description	t (sec)
I	Bare Hull	19.73
II	SR1 – Conventional	19.50
III	SR1 – Small Rectangular	19.44
IV	SR1 – Large Rectangular	19.61
V	SR1 – Small Triangular	19.47
VI	SR1 – Large Triangular	19.54
VII	SR2 – Small Rectangular	19.24
VIII	SR2 – Large Rectangular	19.47
	SR1 – Optimal	19.33
	SR2 – Optimal	19.14

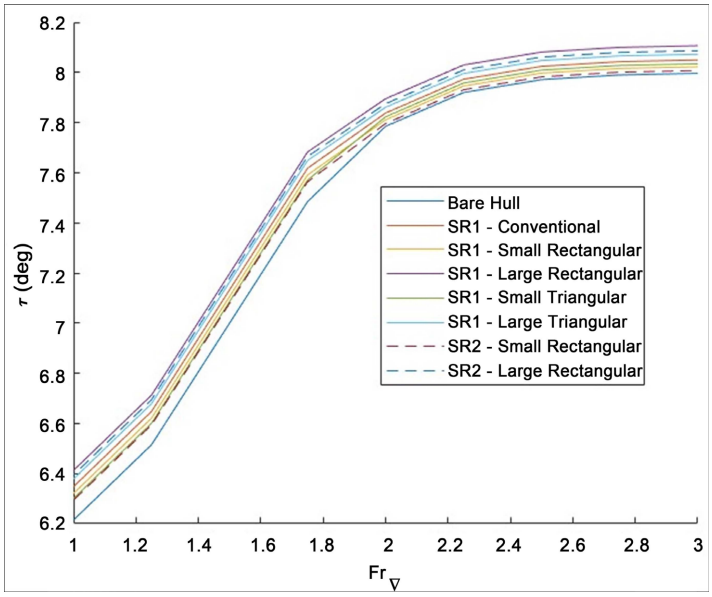

Figure 11. Trim angle variation at hump speeds.

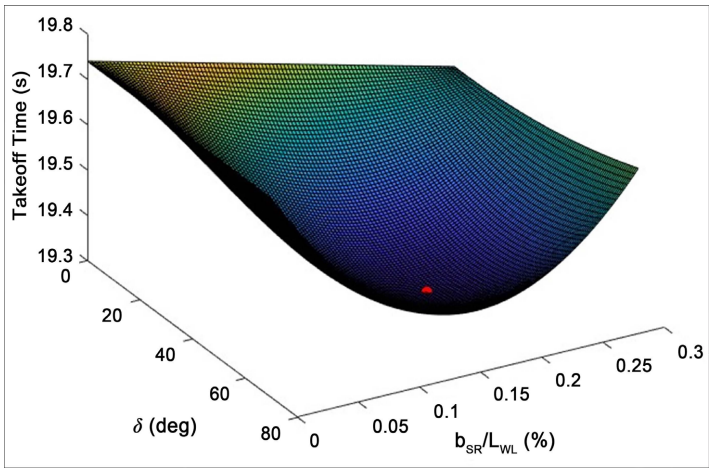

Figure 12. Takeoff time of an amphibian hull with short spray rails.

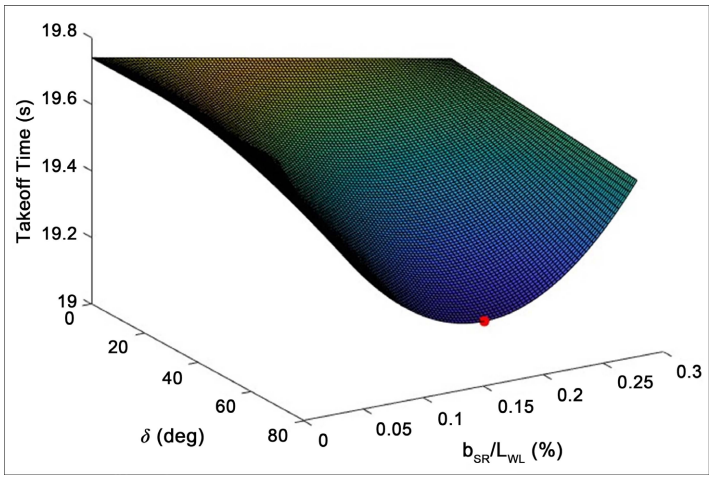

Figure 13. Takeoff time of an amphibian hull with long spray rails.

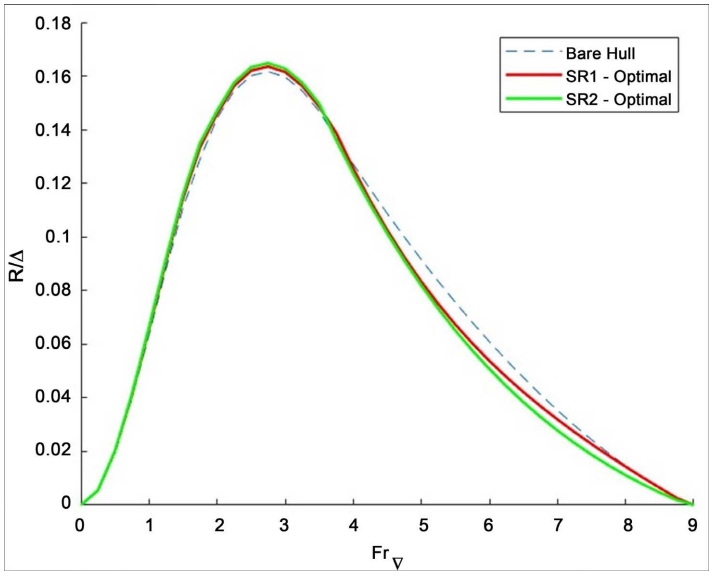

Figure 14. Water resistance of optimal spray rails compared to bare hull based on lowest takeoff time.

curves for the optimal spray rails and the bare hull. Upon a closer look, the optimal short spray rails increase the resistance by up to 3.32%, while the optimal long spray rails increase it by up to 4.58% at displacement speeds. The peak resistance increase is at 1.18% for optimal SR1 and 2% for optimal SR2 as can be inferred from **Figure 15**. The resistance increases at hump speeds as shown in **Figure 16** and drops at planing speeds by a maximum of 11.72% with optimal SR1 $\left(Fr_{\nabla}=6\right)$ and 21.22% with optimal SR2 $\left(Fr_{\nabla}=7\right)$ as shown in **Figure 17**. Spray edge breakage could be predicted to be more for the long spray rails at planing speeds due to them being extended until the step, hence, the resistance was reduced more than the short spray rails. On the other hand, the short spray rails keep the increased resistance at displacement and hump speeds lower than the long spray rails because the length of the spray rails submerged in the water could potentially cause an increase in frictional resistance. **Figure 18** brings the comparison for water resistance of optimal short spray rails with other short spray rail configurations for $0<Fr_{\nabla}<9$.

The conventional short spray rails cause a 4.26% increase in resistance at displacement speeds (**Figure 19**) and a 1.1% increase in resistance at hump speeds (**Figure 20**) compared to the bare hull, which is very similar to the results obtained from the optimal condition for short spray rails. Considering a constant spray rail width with a varying angle, the rectangular spray rails show a 3.27% average decrease in resistance compared to a 3.39% average decrease by the triangular spray rails during displacement. However, the triangular spray rails reduce the hump resistance by 1.16% compared to 1.18% by rectangular spray rails. While these are minor differences, it is crucial to note that the deflection angle plays a vital role in the resistance and spray suppression, the larger the deflection angle, the lower the spray height at displacement. In addition, the triangular spray rails are sharper than the rectangular spray rails, which is essential

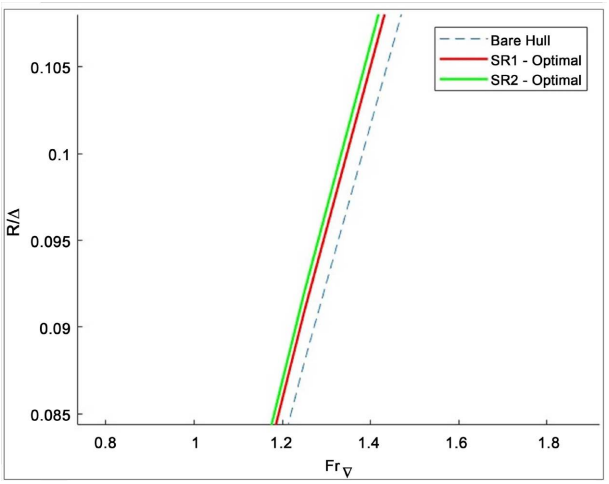

Figure 15. Water resistance of optimal spray rails compared to bare hull at displacement speeds.

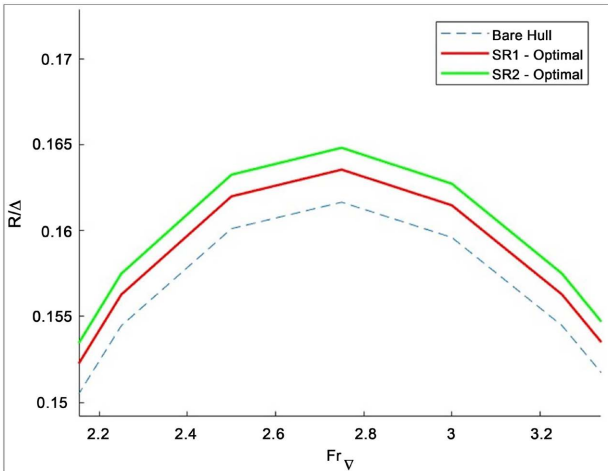

Figure 16. Water resistance of optimal spray rails compared to bare hull at hump speeds.

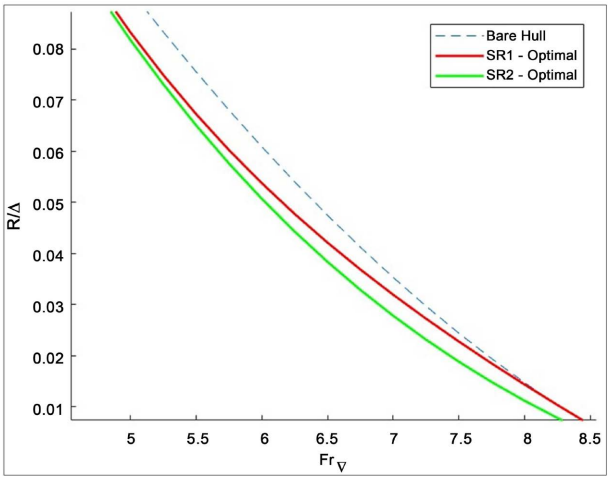

Figure 17. Water resistance of optimal spray rails compared to bare hull at planing speeds.

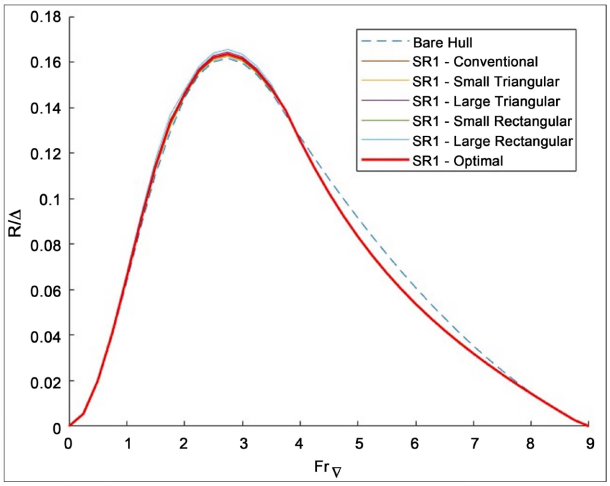

Figure 18. Water resistance of optimal short spray rails compared to other short spray rail configurations.

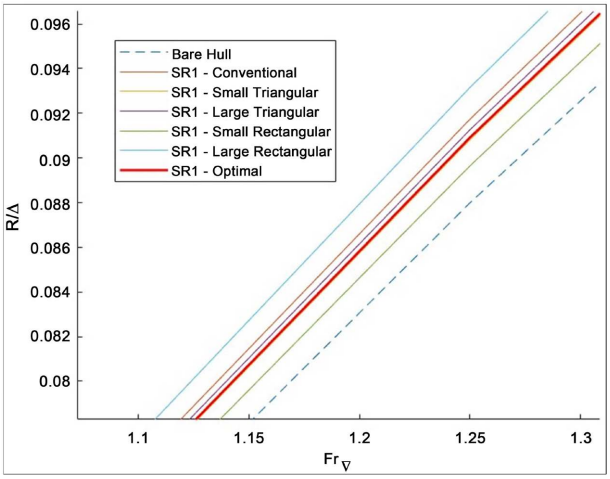

Figure 19. Water resistance of short spray rail configurations at displacement speeds.

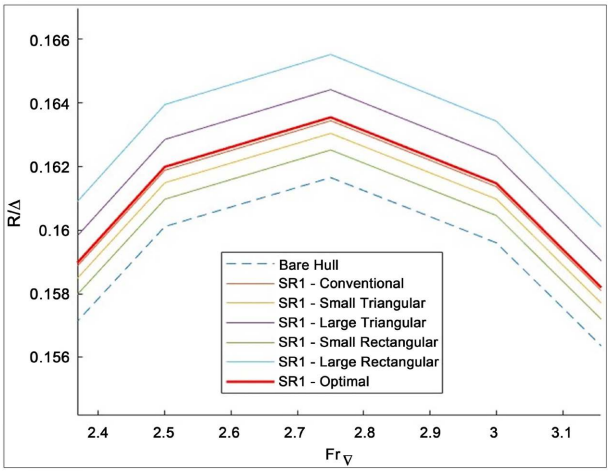

Figure 20. Water resistance of short spray rail configurations at hump speeds.

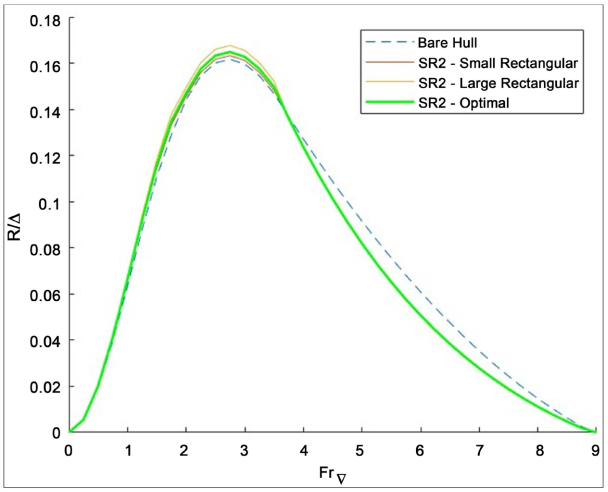

Figure 21. Water resistance of optimal long spray rails compared to other long spray rail configurations.

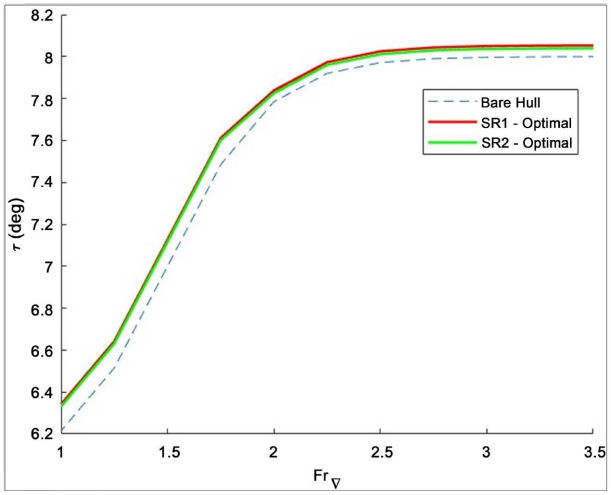

Figure 22. Trim of optimal spray rails compared to bare hull based on lowest takeoff time.

to ensure minimum water contact on the hull. This factor causes the resistance to increase for triangular rails only slightly with increasing width at both displacement and hump speeds.

In contrast, a big jump in resistance is seen for small and large rectangular rails. Another point of interest is that the SR1 resistance curves merge at planing speeds, which means that the spray rails' shape, angle, and width do not seem to affect the resistance. A similar comparison in resistance was recorded for long spray rail configurations as well, which can be seen in Figure 21.

The trim is another factor that changed for the optimal configurations; a maximum of 2.12% increase in trim was observed for optimal SR1 at the start of displacement but reduced to a mere 0.15% increase at the start of planning, which remains until takeoff. A similar trend was observed for optimal SR2, where the trim increase reached a maximum of 1.93% (Figure 22). An inference

can be made from this trend, which is that the longitudinal orientation of the amphibian hull does not change drastically with the addition of spray rails. Furthermore, the long spray rails were more effective in maintaining the trim than the short spray rails.

6. Conclusion

According to the analysis presented in this paper, the spray rail additions successfully reduced the resistance and takeoff time while maintaining a steady trim throughout the takeoff run of the amphibian hull. The tested spray rail configurations for the amphibian hull provided a better understanding of how spray rails affect the takeoff performance for flying boats and amphibians. While the selected configuration for the Seamax M22 hull seems to be the best option for the reasons stated above, water tank tests are necessary to attest its behavior. While the spray rail geometry influences the hydrodynamic characteristics of the hull, it was found that these effects are small, but it can be significantly larger for hulls larger than the Seamax M22. This analysis could then benefit future amphibian designs with larger hulls that have more transport capabilities than the Seamax M22, such as amphibian fire fighters with large payload capability. Some uncertainties in the data can be addressed in a future study since the results were replicated, scaled, and interpolated from various sources. The use of CFD is one option to attest the found results; however, water tank tests provide more accurate and realistic results, as previously mentioned. This study neglects the effects of external factors like crosswinds, rough waves, and salinity, which can be considered by exploring this topic further.

Conflicts of Interest

The authors declare no conflicts of interest regarding the publication of this paper.

References

[1] Gudmundsson, S. (2013) Appendix C3: Design of Seaplanes. In *General Aviation Aircraft Design: Applied Methods and Procedures*, Elsevier, Inc., Amsterdam.

[2] De Havilland Aircraft of Canada, Ltd. (2022) De Havilland Aircraft of Canada Limited Launches DHC-515 Firefighter. https://dehavilland.com/en/news/posts/de-havilland-aircraft-of-canada-limited-launches-dhc-515-firefighter

[3] Pike, D. (2020) Spray Rails and Chines. BoatTEST. https://boattest.com/article/spray-rails-and-chines

[4] Lakatoš, M., Sahk, T., Andreasson, H. and Tabri, K. (2022) The Effect of Spray Rails, Chine Strips and V-Shaped Spray Interceptors on the Performance of Low Planing high-Speed Craft in Calm Water. *Applied Ocean Research*, **122**, Article 103131. https://doi.org/10.1016/j.apor.2022.103131

[5] Savitsky, D. and Morabito, M. (2011) Origin and Characteristics of the Spray Patterns Generated by Planing Hulls. *Journal of Ship Production and Design*, **27**,

63-83. https://doi.org/10.5957/jspd.2011.27.2.63

[6] Müller-Graf, B., Holden, K.O., Faltinsen, O.M. and Moan, T. (1991) The Effect of an Advanced Spray Rail System on Resistance and Development of Spray of Semi-Displacement Round Bilge Hulls. *FAST '91, 1st Intl. Conf. Fast Sea Transportation,* **1**, 125-141.

[7] Clement, E.P. (1945) Reduction of Planing Boat Resistance by Deflection of the Whisker Spray. David Taylor Model Basin, Department of The Navy, Report No. 1929.

[8] Hugli Jr., W.C. and Axt, W.C. (1951) Hydrodynamic Investigation of a Series of Hull Models Suitable for Small Flying Boats and Amphibians. NACA TN-2503, Stevens Institute of Technology.

[9] Suydam, H.B. (1952) Hydrodynamic Characteristics of a Low-Drag Planing-Tail Flying-Boat Hull. NACA TN-2481, Langley Aeronautical Laboratory.

[10] Clement, E.P. (1964) Effects of Longitudinal Bottom Spray Strips on Planing Boat Resistance. David Taylor Model Basin, Department of The Navy, Report No. 1818.

[11] Savitsky, D., DeLorme, M.F. and Datla, R. (2007) Inclusion of Whisker Spray Drag in Performance Prediction Method for High-Speed Planing Hulls. *Marine Technology and SNAME News,* **44**, 35-56. https://doi.org/10.5957/mt1.2007.44.1.35

[12] Frediani, A., Cipolla, V., Oliviero, F., Lucchesi, M., Lippi, T. and Luci, S. (2013) A New Ultralight Amphibious PrandtlPlane: Preliminary CFD Design of the Hull. *Aerotecnica Missili & Spazio*, **92**, 77-86. https://doi.org/10.1007/BF03404665

[13] Yousefi, R., Shafaghat, R. and Shakeri, M. (2013) Hydrodynamic Analysis Techniques for High-Speed Planing Hulls. *Applied Ocean Research*, **42**, 105-113. https://doi.org/10.1016/j.apor.2013.05.004

[14] Locke Jr., F.W.S. (1994) General Resistance Tests on Flying-Boat Hull Models. NACA ARR-4B19, Stevens Institute of Technology.

[15] Locke Jr., F.W.S. (1945) General Main Spray Tests on Flying-Boat Hull Models. NACA ARR-5A02, Stevens Institute of Technology.

[16] Begovic, E. and Bertorello, C. (2012) Resistance Assessment of Warped Hull Form. *Ocean Engineering*, **56**, 28-42. https://doi.org/10.1016/j.oceaneng.2012.08.004

[17] Celano, T.III. (1998) The Prediction of Porpoising Inception for Modern Planing Craft. USNA Trident Report No. 254.

[18] Larsson, L., Eliasson, R.E. and Orych, M. (2014) Principles of Yacht Design. 4th Edition, Adlard Coles Nautical, London.

[19] Rosario, M. (2022) Pilot Operating Handbook and Aircraft Flight Training Supplement: Seamax M22. Seamax Aircraft Ltd., Rev. No. 07.4.

[20] Dinc, A. and Otkur, M. (2020) Emissions Prediction of an Aero-Piston Gasoline Engine during Surveillance Flight of an Unmanned Aerial Vehicle. *Aircraft Engineering and Aerospace Technology*, **93**, 462-472. https://doi.org/10.1108/AEAT-09-2020-0196

Nomenclature

Δ = aquatic forces
C_{Δ} = load coefficient
w = specific gravity of water
g = gravitational acceleration
β = deadrise angle
β_{SR} = spray rail deadrise angle
∇ = displaced volume
R = water resistance
R_f = frictional resistance
R_d = dynamic resistance
δR = change in resistance
Fr_{∇} = Froude displacement number
τ = trim angle
τ_1 = trim angle at start of takeoff run
τ_2 = trim angle at end of takeoff run
$\delta\tau$ = change in trim angle
C_V = speed coefficient
C_R = resistance coefficient
T = available thrust
$T_{72\%}$ = thrust at 72% maximum continuous power
D = air drag
V = speed
a = acceleration
t = total takeoff time
b = maximum beam length
b_s = beam length at step
L = Lift
L_{SR} = spray rail lift
L_f = forebody length
L_a = afterbody length
L_{WL} = length of waterline
l_{SR} = spray rail length
h_s = step height
λ = linear scaling factor
b_{SR} = spray rail width
δ_{SR} = spray rail deflection angle

Subscripts

M = model
i = iteration number